Experimental Investigation of Combustion Efficiency of Air-Augmented Rockets

Zhang Zhongqin,* Zhang Zhenpeng,† Tao Jinfu† and Feng Wenlan*
Beijing Institute of Aeronautics and Astronautics, Beijing, China

This paper reports the results of an experimental study concerned with the mixing and combustion processes in air-augmented rockets. A combustor assembly consisting of the primary rocket and the secondary, constant-area combustion chamber were utilized to simulate a typical tactical missile. Several different configurations of the primary chamber rocket nozzles have been designed and tested in order to evaluate the mixing in the after-burning combustion chamber. On the basis of the experimental results, the secondary combustor using the subsonic primary nozzle with multiple jets has been shown to achieve the highest combustion efficiency, about 30% greater than that of the single-sonic or supersonic nozzles. Instrumentation was also provided for measurements of the pressures and velocities of the ducted flow. These measurements provide a basis for an understanding of the combustion process.

Nomenclature

A	= cross-sectional area
C_p	= heat capacity at constant pressure
D	= duct diameter
F	= thrust
F_m	= thrust measured in tests
H_u	= heating value of complete combustion
L_o	= stoichiometric ratio of air to fuel
$\dot{m}_s, \dot{m}_p, \dot{m}_T, \dot{m}_{T'}$	= mass flow rate of secondary flow, primary gas flow, kerosine injected into the heater, kerosine burned in the duct, respectively
Q_p	= heating value in the primary rocket
R	= gas constant
T_a	= ambient temperature
T_s^*	= stagnation temperature of second flow at the inlet of the ram chamber
T_3^*	= stagnation temperature at the inlet of the secondary nozzle
X	= axial distance measured from the primary nozzle exit plane
Y	= radial distance measured from the centerline
α	= ratio of measured to stoichiometric Air/Fuel
λ	= velocity coefficient

Subscripts

a	= ambient
H	= ambient condition at altitude H
m	= measured
p	= primary
s	= secondary
T	= kerosine
w	= wall
2	= primary nozzle exit plane
3	= secondary nozzle inlet plane
4	= secondary nozzle exit plane

Received April 9, 1985; presented as Paper 85-1314 at the AIAA/SAE/ASME/ASEE 21st Joint Propulsion Conference, Monterey, CA, July 8-10, 1985; revision received Feb. 19, 1986.

*Associate Professor.
†Lecturer.

Introduction

AIR-breathing ducted rockets of the type shown in Fig. 1 offer higher values of specific impulse than solid propellant motors. These ducted rockets are relatively simple compared with ramjets because a liquid fuel feed system is not required. Recently, it has been shown[1,2] that a renewed interest exists in the application of a ramjet type of propulsion device for the new generation missiles.

In these ducted rockets, the combustion products of the primary chamber containing gaseous and particulate fuels are injected into an after-burning combustor. The primary nozzle geometry significantly influences mixing and combustion of the primary combustion products in the primary jet with the oxidizer of the secondary airstream. Therefore, the combustion efficiency can be significantly improved by the selection of a primary nozzle geometry which provides better mixing.

An extensive literature review of experimental results related to mixing and combustion of particle-laden streams was reported previously.[3,4,5] However, little experimental data for a real size air-augmented rocket were reported.

It is generally known from earlier test results that:

1) The metallized fuel-rich propellant formulation not only considerably affects the combustion performance of the primary chamber, but also that of the secondary chamber.

2) The secondary chamber pressure is determined by the design speed and altitude of the missile according to its mission. Chamber pressure, in turn, strongly affects the air-to-fuel ratio and the mixing characteristics.

3) The secondary duct length as well as the injection angle and location leave a marked influence on mixing and combustion performance.

The primary objective of this research effort was to experimentally explore the approach to achieving improved combustion efficiency in ducted rockets while extending their reliable operation range. The present study did accomplish its primary goal, that is, to provide the designers with useful data.

Experimental Arrangement

The experimental apparatus is shown schematically in Fig. 2. the secondary air-supply system was constructed so that flight speed and altitude can be simulated. The upstream air was heated in a kerosine burner to about 500 K prior to entering the mixing duct.

The air flow rate was measured using the sonic throat method[6] with a throat diameter of 82 mm. A large plenum chamber was incorporated upstream from the sonic throat to

stabilize the air flow. This assembly was mounted vertically to the test stand, so that the inlet momentum of the air entering the chamber was minimized. Furthermore, the accuracy of thrust measurement was improved. An adequate radial gap between the plenum neck and the air pipe inner wall was provided to make the test rig independent of the forces and movement of the air supply pipelines.

The air stream flows into an annular manifold and is subsequently injected into the mixing chamber through four inlet ports at an injection angle of either 40, 60 or 90 deg measured from the centerline. The injection area is maintained the same for all injection angles. The secondary chamber could be assembled from several different lengths bolted together. As a result, the required length-to-diameter ratio ranging from 2 to 10 was easily obtained in the test series.

Primary Chamber

The general configuration of the solid propellant motor with its interchangeable nozzle is illustrated in Fig. 3. The end-burning grain of aluminized fuel-rich propellant had a length of 150 mm and a diameter of 212 mm. The nozzle and its injection head were made of copper-infiltrated tungsten which provided cooling as the infiltrant vaporized at high temperature to minimize nozzle erosion. the ignition squib containing 12 g of polytetrafluoroethylene, 12 g of magnesium powder, and 6 g of black powder successfully ignited the grain.

Instrumentation

The system was instrumented for measurement of pressure, temperature, thrust and kerosine flow rate. Figure 4 illustrates the basic sequential steps for the acquisition of the required measurements. In addition to the measurement of the steady state parameters outlined above, transient data were also measured with the aid of a magnetic tape analog recorder/reproducer, ultraviolet oscillograph and a dynamic pressure measurement system.

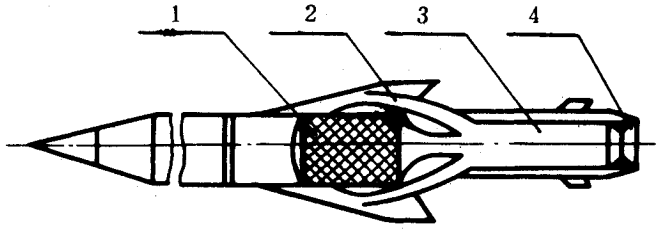

Fig. 1 Model of air-augmented rocket: 1) solid-propellant rocket, 2) air inlet, 3) ram chamber, and 4) nozzle.

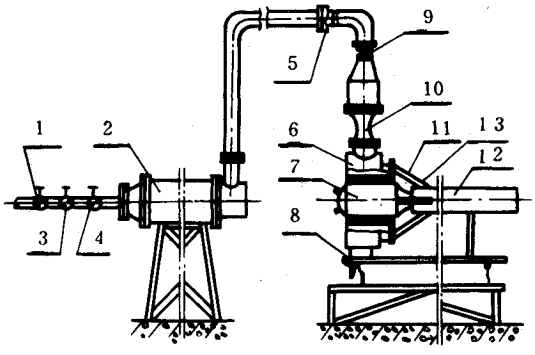

Fig. 2 Schematic diagram of test facility: 1) valve, 2) heater, 3) servo-valve, 4) regulator, 5) flexible joint, 6) plenum chamber, 7) rocket motor, 8) thrust rig, 9) parallel gap, 10) secondary chamber, and 13) temperature measurement.

Cold-Flow Tests

As a first step toward preliminary evaluation of the experimental setup, a series of cold-flow tests were performed.

Mixing characteristics were determined for a primary air jet and a nonparallel (40 deg injection angle measured from the center line), four-inlet secondary stream of unvitiated air. Four primary air nozzles, both sonic and supersonic, having angles of either 0, 15 or 30 deg were used in the preliminary evaluation. Also, a nozzle having 13 jets was investigated.

Figures 5 and 6 show typical radial and axial pressure profiles of the secondary stream in the absence of the central primary flow. As can be seen from the plots, there was no observable variation of either radial or axial static pressure in the secondary duct. Accordingly, it can be assumed that the secondary flow becomes parallel near the injection exit plane.

Figs. 7 and 8 illustrate the radial static and total axial pressure profiles of the primary air stream at different axial stations in the absence of the secondary injection. The probe rake which made the measurements was installed horizontally. The nozzle used had four injection orifices of 8 mm diameter at an angle of 15 deg.

The confined flowfield was appreciably different from that of a free jet structure. The results indicate that the static pressure increased slightly with radial distance in the fore-end of the chamber. It was evident that the nonparallel airflow was very rapidly turned to the axial direction. An increase of static pressure along the chamber was also observed. It was to be expected that the total pressure decreased radially only at distances close to the nozzle exit plane.

The effect of nozzle configuration on jet mixing was experimentally studied. The results, typical of a number of tests, are shown in Figs. 9 and 10. The core velocity at $X/D=1$ was much higher (350 m/s) compared to the velocity (80 m/s) in

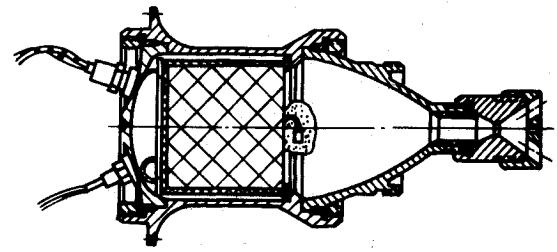

Fig. 3 Solid propellant motor.

Table 1 Properties of the propellant and combustion products

Propellant	
HTPB, % by wt.	17
AP, % by wt.	50
Al, % by wt.	20
Mg, % by wt.	3
Heating value Hu (of complete combustion), KJ/kg	18225
Heating value Q_p (in primary rocket), KJ/kg	3638
Burn rate r, mm/s	5-7
Gas generator	
Run duration t, s	19-24
Pressure P_p, MP_a	7.0924
Flow rate $\dot{m}_p$, kg/s	0.40
Combustion chemistry	
Flame tempertuare T_p^*, K	2400
Specific heat c_{pp}, KJ/kgK	1.795
Specific heat ratio k	1.24
Gas constant R, KJ/kg K	0.3506
Characteristic velocity C*, m/s	1400
Stoichiometric A/F ratio L_o	2.812

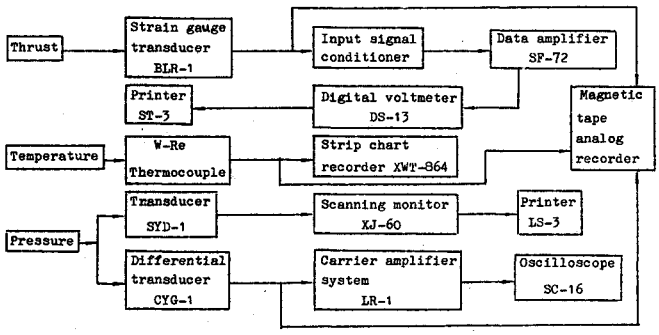

Fig. 4 Schematic diagram of test facility.

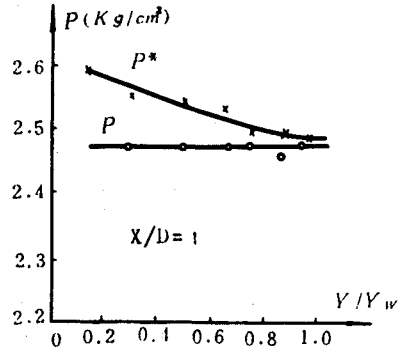

Fig. 5 Radial secondary flow profiles of static and total pressure.

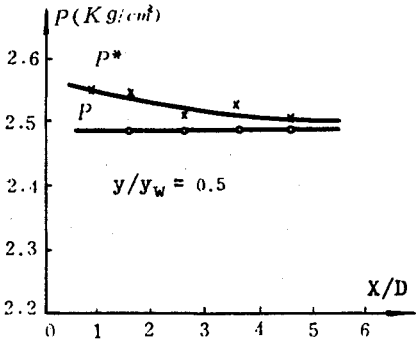

Fig. 6 Axial secondary flow profiles of static and total pressure.

the vicinity of the wall. The mixer flowfield approached uniform flow across the duct at distances as far as $X/D=5.8$ downstream. Little improvement was achieved with a supersonic central flow or for a nozzle with four 8 mm diameter parallel jets. For that configuration, the central flow velocity was 250 m/s, while the outer flow velocity was only 60 m/s at $X/D=1$.

The resulting velocity distributions for both 15-degree angle jets and 13-orifice injection were similar and are shown in Fig. 10. Uniformity in velocity distribution was rapidly reached at distance $X/D=2.8$ and downstream. It was observed that the orifices of the injection head with 13 jets were frequently clogged with slag during firing.

From the standpoint of the mixing rate, the 30-deg injection angle was ideal. The maximum central flow velocity was about 120 m/s, while the velocity of the outer flow at $X/D=1$ was 80

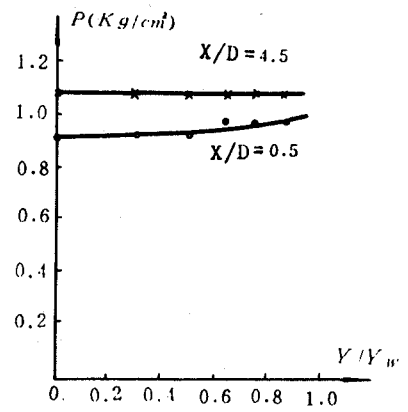

Fig. 7 Static pressure profiles of primary air stream.

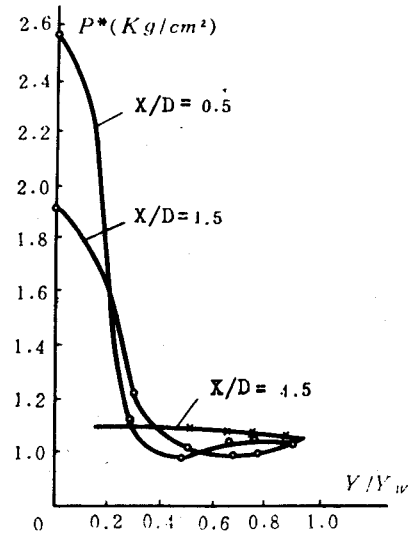

Fig. 8 Total axial pressure profiles of primary air stream.

m/s. The centerline velocity at $X/D=5$ was even less than the outer flow velocity.

It was found during firing runs that a large injection angle has the critical disadvantage of bringing the hot exhaust gases into direct impact onto the duct wall possibly ablating material from the wall surfaces. This adverse effect completely offset the enhanced mixing rate caused by the strong impingement of the two streams. A 15-deg injection angle provided a tradeoff between good mixing and gaseous impact on the wall. The 15-deg injection angle was further proved successful in the combustion test series.

Mixing characteristics as determined from the cold flow experiments are of primary importance for indicating the best configuration for achieving higher combustion efficiency.

Complete combustion can be realized provided the oxygen involved in the airflow has enough time to react with the fuel-rich primary exhaust in a high temperature combustor. Therefore, the primary flow velocity should not be too high in order to extend its residence time.

Combustion Efficiency

The fuel-rich products exhausted from the motor contained high loadings of unburned aluminum agglomerates. Since the oxidizing potential of gases was high, it is essential that efficient after-burning in the secondary chamber takes place, thereby, permitting reasonable combustion efficiencies to be achieved. Aluminum particles can be completely burned in an oxidizing environment if the temperature is higher than 2300 K

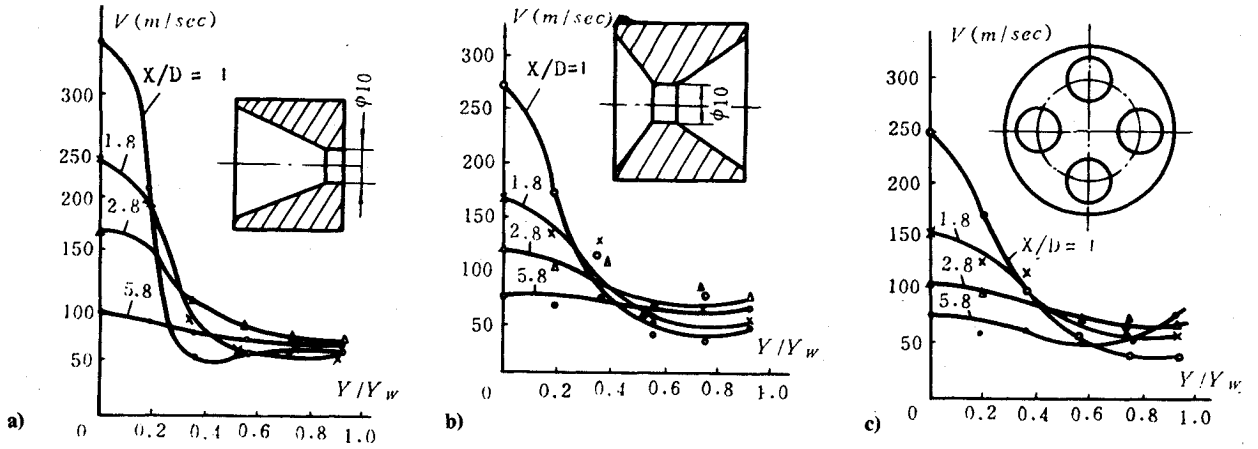

Fig. 9 Velocity profiles of a) sonic nozzle, b) supersonic nozzle, and c) nozzle with four 8mm parallel jets.

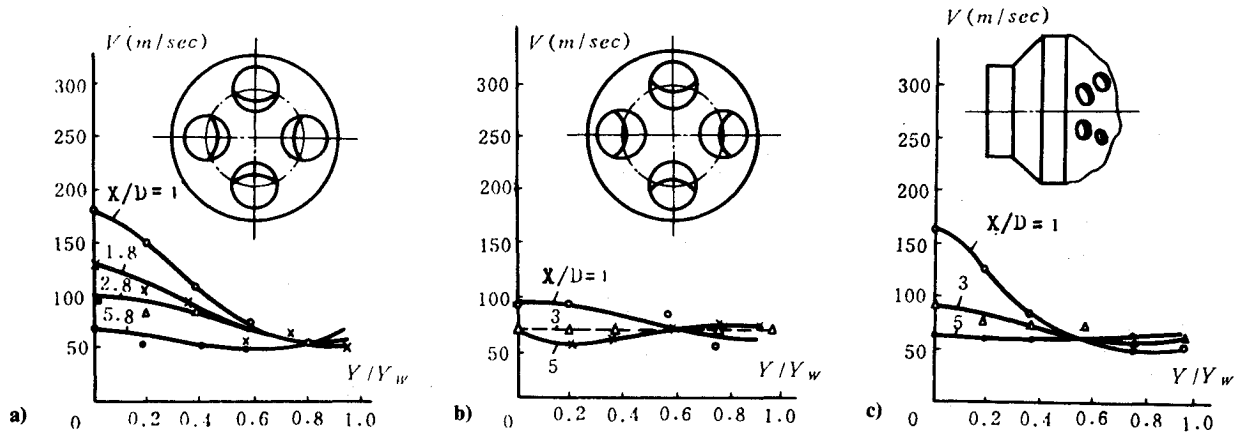

Fig. 10 Velocity profiles of nozzle with a) four jets at 15-degree angle, b) four jets at 30-degree angle, and c) 13-orifice injection head.

Table 2 Experimental data with sonic (runs 1 and 2) and supersonic (runs 3, 4 and 5) nozzles

	Run				
	1	2	3	4	5
P_a(MPa)	0.1015	0.1009	0.1014	0.1013	0.1010
p_a^*(MPa)	0.3594	0.3537	0.3598	0.3478	0.3481
p_3^*(MPa)	0.2486	0.3062	0.2980	0.3132	0.2673
p_p^*(MPa)	6.2784	7.0142	5.8860	5.6898	4.0221
α	3.286	2.998	2.753	2.850	3.799
η	0.5664	0.4804	0.4758	0.5787	0.5482

Table 3 Experimental data of subsonic nozzles with multiple jets

	Run				
	1	2	3	4	5
P_a(MPa)	0.0977	0.1007	0.1005	0.1014	0.1006
p_a^*(MPa)	0.3637	0.3602	0.3545	0.3678	0.3684
p_3^*(MPa)	0.3009	0.3037	0.2967	0.3303	0.3023
p_p^*(MPa)	6.3765	8.5347	6.1607	8.0442	7.3575
α	3.347	2.659	3.311	2.833	2.920
η	0.7716	0.6926	0.7467	0.6950	0.6803

Table 4 Slag compositions

	Al	Al_2O_3	C	Fe
Sonic nozzles	48	48.77	2	1.23
Nozzles with multijet	0	95.80	2.91~2.95	1.27

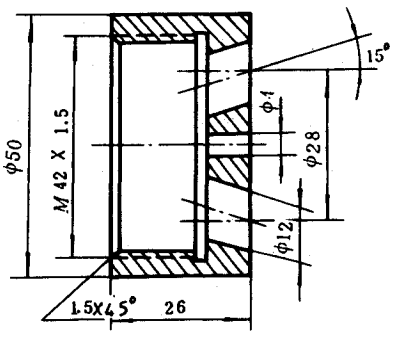

Fig. 11a Injection heads with central orifice.

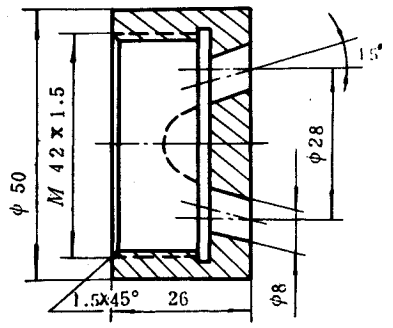

Fig. 11b Injection heads without central orifice.

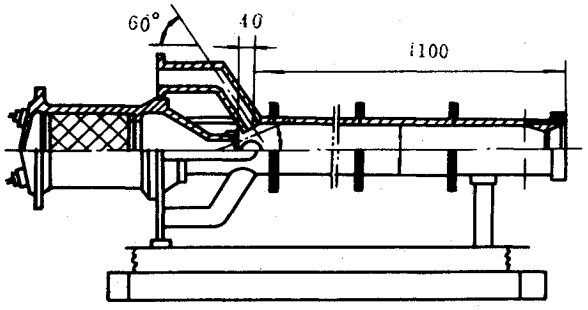

Fig. 12 Schematic of the after-burning chamber.

which assures the melting of the protective Al_2O_3 shielding layer. In addition, the particle residence time t_s should be longer than the ignition delay time t_i.

In the present study, 200% excess air was supplied. The velocity coefficient λ_p of the primary flow was as high as 2.037 for the supersonic rocket nozzle, whereas the velocity coefficient of particles was less than λ_p as the particle temperature approached 2400 K. The ignition delay time can be approximated[7] as $t_i = 0.32$ ms if 12 μm aluminum particle size is as assumed. The time required for gases passing across a length of 10 cm is about 0.05 ms, and $t_s = 0.07$ ms for particles when the two-phase time lag is considered. The particle residence time t_s becomes 0.16 ms if a sonic ($\lambda_p = 1$) nozzle is used. In both cases, t_s is much less than t_i and, therefore, the subsonic nozzles with multiple 15-deg jets employed in this study have been found to work best after test firing a series of motors with supersonic and sonic nozzles (Fig. 10).

The injection heads of the nozzle are shown in Fig. 11. It was found that the Fig. 11b configuration resulted in a thick buildup of slag at the center of the back surface of the nozzle. A central bore was thus made to remove the slag accumulation as shown in Fig. 11a.

Figure 12 illustrates the relative position of the primary nozzle to the secondary air inlet ports. The rocket exhaust gases impinge upon the secondary airflow when a four-jet nozzle head is used.

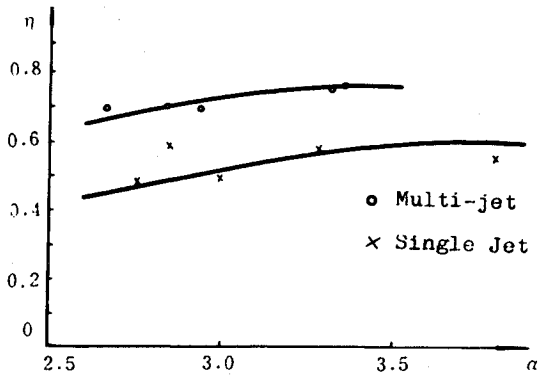

Fig. 13 Combustion efficiency of different primary nozzles.

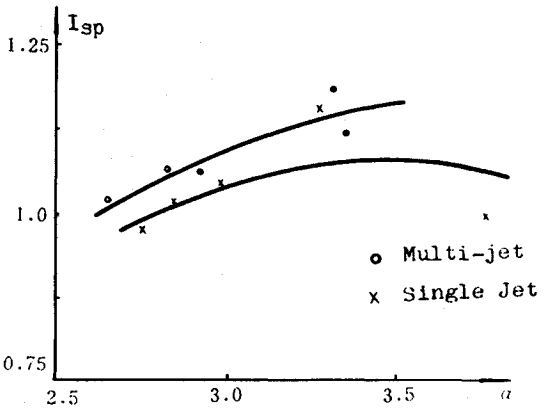

Fig. 14 Specific impulse of different primary nozzles.

The following assumptions were made for data reduction: 1) The flow is steady, one dimensional and single-phase. Mean parametric values at each chamber cross-section have been used. 2) Heat losses are negligible; and 3) dissociation does not occur.

The following equations have been used for computing thrust F, specific impulse I_s and combustion efficiency η, respectively:

$$F = F_m - \dot{m}V_H + A_4(P_a - P_H)$$

$$Is = F/\dot{m}$$

$$\eta = \frac{1}{Hu - Q_p}\left\{\left(1 + \alpha L_o + \frac{\dot{m}_T}{\dot{m}_p}\right)C_{p3}(T_3^* - T_a) - [Q_p + L_o C_{ps}(T_s^* - T_a) + 43120\,\dot{m}_T'/\dot{m}_p]\right\}$$

The stagnation temperature at the inlet of the secondary nozzle T_3^* is

$$T_3^* = (k - 1/2kR\dot{m})[F_m - A_4(p_4 - p_a)]^2[1 - (p4/p_3^*)^{k-1/k}]^{-1}$$

The amount of kerosine burned is

$$\dot{m}_T' = [43120\,\dot{m}_T - \dot{m}_s C_{ps}(T_s^* - T_a)/C_{pT}(T_s^* - T_s) + 43120]$$

The following relationships and values are also used:

$$L_o = \dot{m}_s/\dot{m}_p \qquad c_{ps} = 1.005\ \text{KJ/kgK}$$

$$\dot{m} = \dot{m}_T + \dot{m}_p + \dot{m}_s \qquad c_{p3} = 1.247\ \text{KJ/kgK}$$

$$\dot{m}_T = 0.02\ \text{kg/s}$$

A summary of test conditions and experimental results for each of the 5 test runs conducted is shown in Tables 2 and 3, while Figs. 13 and 14 show the corresponding performances. The air injection angle in each of these cases is 60 deg.

It is clear from these results that the combustion efficiency of multiple injection nozzles is about 30% higher than that of sonic or supersonic conventional nozzles. Moreover, the values of the specific impulse increase by as much as 8%.

Conclusions

Experimental results indicated that the configuration of the primary nozzle of an air-augmented rocket has a drastic influence on its after-burning performance. Multiple injection nozzles can enhance the mixing process of the primary with the secondary airflow and decelerate the exhaust velocity from sonic or supersonic to subsonic, thus, prolonging the residence time of the primary exhaust products. The impingement of the primary jets with the nonparallel airstream causes the formation of a recirculation region; therefore, the mixing effect is enhanced.

The analysis of slag taken from the P_3^* probe tip revealed that the amount of the unburned aluminum in the case of single primary jet was much more than that in the multijet case (Table 4). Half of the slag was comprised of unburned aluminum, while no aluminum was found in the slag for the multijet nozzles. The same trend was shown from the plume observation that dark red flaring particles were entrained in the flame indicating that unburned aluminum particles were being ejected from the single sonic motor nozzle. The flame of the multijet nozzle configuration was, on the other hand, merely bright without the appearance of the dark red particles.

Acknowledgments

The experiments were conducted at the Jet Propulsion Laboratory in the Department of Propulsion. The authors wish to express their appreciation to Prof. J. R. Osborn for reviewing the paper.

References

[1]Thomas, A. N., "Return of the Ramjet," *Astronautics and Aeronautics*, Jan. 1984.

[2]Thomas, A. N., "New Generation Ramjets—A Promising Future," *Astronautics and Aeronautics*, June 1980.

[3]Smoot, L. D., "Particle-gas Mixing in Air-Breathing Ducts with Nonparallel Multiple-Port Air Injection," AIAA Paper 75-246, Jan. 1975.

[4]Schadow, K., "Fuel-Rich, Particle-Laden Plume Combustion," AIAA Paper 75-245, Jan. 1975.

[5]Kushner, D. S., "Combustion Rate Processes in the Secondary Combustion of an Air-Augmented Solid Propellant," AD716330, Oct. 1970.

[6]Stanly, Q., "Accuracy of Gas Flow Measurements Using the Sonic Throat Method," NASA CR 99127.

[7]Friedman, R. and Macek, A., "Combustion Study of Single Aluminum Particles," *Proceedings of the 9th International Symposium on Combustion*, 1963.